Universality in three-dimensional Ising spin glasses: A Monte Carlo study

Helmut G. Katzgraber,[1] Mathias Körner,[1] and A. P. Young[2]
[1]*Theoretische Physik, ETH Zürich, CH-8093 Zürich, Switzerland*
[2]*Department of Physics, University of California, Santa Cruz, California 95064, USA*
(Received 8 February 2006; revised manuscript received 20 April 2006; published 23 June 2006)

We study universality in three-dimensional Ising spin glasses by large-scale Monte Carlo simulations of the Edwards-Anderson Ising spin glass for several choices of bond distributions, with particular emphasis on Gaussian and bimodal interactions. A finite-size scaling analysis suggests that three-dimensional Ising spin glasses obey universality.

DOI: 10.1103/PhysRevB.73.224432 PACS number(s): 75.50.Lk, 75.40.Mg, 05.50.+q

I. INTRODUCTION

One of the cornerstones of the theory of critical phenomena is the concept of universality, according to which the values of many quantities, such as critical exponents, do not depend on microscopic details but only on a few broad features such as the dimensionality of space and the symmetry of the order parameter. Universality follows from renormalization group (RG) theory, according to which many interactions that could be added to the Hamiltonian are "irrelevant," i.e., do not change the critical behavior. The "ϵ-expansion" implementation of RG has been very successful in predicting which perturbations are actually relevant and which are irrelevant. At least for pure systems, and disordered systems without frustration, numerical simulations seem to be consistent with universality.

However, for systems with both frustration and disorder, known as spin glasses,[1] the situation is less clear. On the one hand, ϵ-expansion calculations as well as high-temperature series expansions[2] for spin glasses imply universality, and, in the opinion of the authors of this paper, there is no *a priori* reason why universality should be less valid for spin glasses than for pure systems. However, as we shall see below, numerical results so far have not been compelling in favor of universality and some groups[3–7] even claim explicitly that universality *is violated*.[8] Unfortunately, it is difficult to obtain accurate critical exponents because there are significant corrections to scaling, there are long equilibration times in Monte Carlo simulations that limit the available system sizes, and all quantities need to be averaged over many realizations of the disorder in order to have small enough error bars.

According to universality, the range of the interactions is irrelevant, as long as it is finite, and so, for example, adding next-nearest-neighbor couplings to a nearest-neighbor model will not change the critical behavior. However, random systems are characterized not just by the strength of first-neighbor, second-neighbor, etc., interactions, but by the *distributions* of these (random) quantities. Hence, even if one restricts oneself to nearest-neighbor interactions, there are many different models characterized by different distributions which are expected to be in the same universality class. In this paper we attempt to answer, through careful simulations, whether this expectation is true for Ising spin glasses in three dimensions.

Many groups have estimated critical exponents for spin glasses for the Edwards-Anderson (EA) Ising spin glass[9] in three dimensions for different disorder distributions, mainly the Gaussian and bimodal ($\pm J$) models. In Table I we present a summary of these results. We also present results from a recent study[10] which uses a three-dimensional diluted Ising spin glass (45% bond occupation). The advantage of such a model is that, due to the dilution, cluster algorithms[11] can be used to study larger system sizes and that corrections to scaling seem to be small[10] when the bonds are drawn from a bimodal distribution. The data in Table I show clearly that there is a large spread in the estimates of the different critical exponents obtained using several different methods, such as series expansions, nonequilibrium relaxation approaches, and finite-temperature Monte Carlo methods combined with a finite-size scaling (FSS) analysis. The spread in the different estimates of the critical exponents ν and η is easily visualized in Fig. 1 where we plot η versus ν. As mentioned above, some groups claim universality is violated,[3–7] but most of the papers do not make this claim, probably because the error bars on the data are usually large. In this paper we aim to test universality in equilibrium more precisely by reducing the error bars.

A major problem with reducing error bars in critical exponents is the presence of corrections to FSS, which means that the scaling expressions used to determine exponents do not work well for small system sizes. For pure systems, several methods have been proposed in an attempt to reduce errors caused by corrections to scaling.

First, try to eliminate the leading correction. In this approach, the model is altered until the operator which gives the leading correction does not appear in the Hamiltonian. This means that its effects will not be felt in *any* calculated quantity. For the three-dimensional Ising ferromagnet, using a "soft-spin" model rather than "hard" ± 1 spins, and varying the coefficient of the fourth-order term in the Hamiltonian, it was possible to eliminate the leading correction to FSS and obtain high-precision values for the critical exponents.[29] We have attempted to do this for the spin glass by (i) choosing different disorder distributions, and (ii) using soft spins as well as hard spins. However, the corrections to scaling for small sizes always had the same sign. Consequently, we have not found a model where we could set the leading correction to zero by fine tuning a parameter in the Hamiltonian. We are not claiming that such a model does not exist; only that we were not able to find it.

TABLE I. Selection of different estimates (chronologically sorted) of the critical temperature T_c as well as the critical exponents computed by different groups for Gaussian (G) as well as bimodal ($\pm J$) random bonds. The estimates show strong variations and often do not agree. Note that T_c is *not* universal, so the issue at hand is whether or not the results for ν and for η agree within the error bars. The results by Jörg (Ref. 10) are for a bond-diluted $\pm J$ spin glass with 45% bond occupation, which is why the estimate of T_c is different than for the standard bimodal spin glass. The results of Toldin *et al.* (Ref. 12) are for a random-anisotropy Heisenberg model (RA) in the strong-anisotropy limit, which is expected to be in the same universality class as the Ising spin glass in three dimensions. The last two rows describe results of the present study and will be described in detail in what follows.

Authors		T_c	ν	η
Ogielski and Morgenstern (Ref. 13)	$\pm J$	1.20(5)	1.2(1)	
Ogielski (Ref. 14)	$\pm J$	1.175(25)	1.3(1)	−0.22(5)
McMillan (Ref. 15)	G	1.0(2)	1.8(5)	
Singh and Chakravarty (Ref. 16)	$\pm J$	1.2(1)	1.3(2)	
Bray and Moore (Ref. 17)	G	1.2(1)	3.3(6)	
Bhatt and Young (Ref. 18)	$\pm J$	1.2(2)	1.3(3)	−0.3(2)
Bhatt and Young (Ref. 19)	G	0.95(5)	1.6(4)	−0.4(2)
Kawashima and Young (Ref. 20)	$\pm J$	1.11(4)	1.7(3)	−0.35(5)
Bernardi *et al.* (Ref. 3)	$\pm J$	1.165(10)		−0.245(20)
	G	0.88(5)		−0.50(4)
Iñiguez *et al.* (Ref. 21)	G	1.02(5)	1.5(3)	
Berg and Janke (Ref. 22)	$\pm J$	1.12(1)		−0.37(4)
Marinari *et al.* (Ref. 23)	G	0.95(4)	2.00(15)	−0.36(6)
Palassini and Caracciolo (Ref. 24)	$\pm J$	1.156(15)	1.8(2)	−0.26(4)
Mari and Campbell (Ref. 4)	$\pm J$	1.20(1)		−0.21(2)
	G	0.86(2)		−0.51(2)
Ballesteros *et al.* (Ref. 25)	$\pm J$	1.138(10)	2.15(15)	−0.337(15)
Mari and Campbell (Ref. 5)	$\pm J$	1.190(15)		−0.20(2)
	G	0.920(15)		−0.42(2)
Mari and Campbell (Ref. 26)	$\pm J$	1.195(15)	1.35(10)	−0.225(25)
Nakamura *et al.* (Ref. 27)	$\pm J$	1.17(4)	1.5(3)	−0.4(1)
Pleimling and Campbell (Ref. 7)	$\pm J$	1.19(1)		−0.22(2)
	G	0.92(1)		−0.42(2)
Jörg (Ref. 10)	$\pm J$	0.663(6)	2.22(15)	−0.349(18)
Campbell *et al.* (Ref. 28)	$\pm J$		2.72(8)	−0.40(4)
Toldin *et al.* (Ref. 12)	RA	0.93(4)	2.4(6)	−0.24(4)
This study	G	0.951(9)	2.44(9)	−0.37(5)
	$\pm J$	1.120(4)	2.39(5)	−0.395(17)

Second, include corrections to FSS in the analysis. Correction terms are characterized by an exponent, which is universal, and an amplitude which is not. Corrections to scaling in a scaling plot, where one attempts to collapse data from different sizes onto a single curve, occur for both the horizontal and vertical axes, see e.g., Ref. 30. Thus, a large number of additional parameters have to be determined from the data when corrections are included. For ferromagnets, where extremely precise data can be obtained for a very large range of sizes, this is possible.[30] However, for spin glasses, the range of system sizes is more limited because of slow dynamics, even though we have used state-of-the-art algorithms and considerable computer time, and the statistics are not as good because there are large variations between different realizations of the disorder. Hence our attempted fits which included corrections to scaling did not determine the parameters well and frequently the nominal "best" fit had extremely large corrections to scaling and unphysical values for the parameters.

Since attempts to eliminate (leading) corrections to scaling and to explicitly incorporate them failed, we resorted to the strategy of just including data for the larger sizes where we expect corrections to be small, and neglecting corrections to scaling. Our main conclusion is that in equilibrium *universality is satisfied*, since results for a particular observable do not appear to depend on the disorder distribution. However, there are still some open questions since *different* observables for a *single* disorder distribution yield estimates of critical exponents which differ by more than the estimated (statistical) error bars. This discrepancy can probably only be

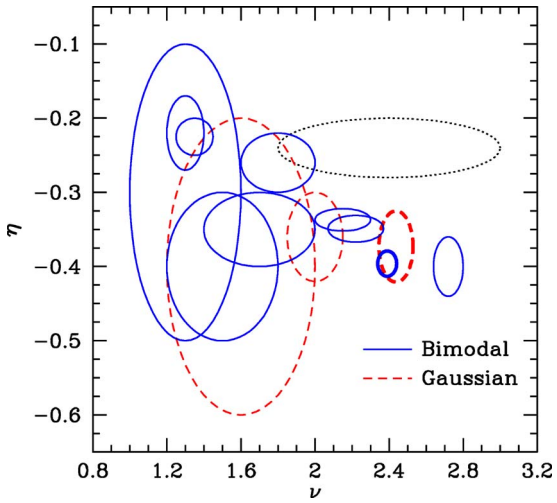

FIG. 1. (Color online) Graphical representation of different estimates of the critical exponents η and ν (taken from Table I). The centers of the ellipses represent the different estimates, and the major axes represent the error bars of the estimates. The data show a considerable spread. The thick lines represent the estimates from the current study. Note that the data from the current study for bimodal (solid lines) and Gaussian (dashed lines) distributions agree within error bars thus providing evidence for universality. The dotted line represents data for a random-anisotropy Heisenberg model in the strong-anisotropy limit (Ref. 12) which is expected to be in the same universality class as the Ising spin glass.

resolved by an analysis incorporating corrections to scaling. Although this does not appear to be possible at present (since the range of sizes is too small) it may be possible in the future if more significantly efficient algorithms can be developed.

The paper is structured as follows: In Sec. II we introduce the model as well as the measured observables and in Sec. III we present details on the Monte Carlo method used. In Sec. IV we discuss the method used to estimate unbiased error bars for the different estimates of the critical parameters. Results are presented in Sec. V, followed by concluding remarks in Sec. VI.

II. MODEL AND OBSERVABLES

A. Edwards-Anderson model

The Hamiltonian of the Edwards-Anderson Ising spin glass[1,9] is given by

$$\mathcal{H} = -\sum_{\langle i,j \rangle} J_{ij} S_i S_j, \tag{1}$$

where the sites i lie on a three-dimensional cubic lattice of size $N=L^3$ and the spins S_i can take values ± 1. The sum is over nearest-neighbor pairs and the interactions J_{ij} are independent random variables. Periodic boundary conditions are applied. In this work we mainly study two paradigmatic cases of the EA model:

• Gaussian-distributed random bonds with zero mean and standard deviation unity

$$\mathcal{P}(J_{ij}) = \frac{1}{\sqrt{2\pi}} e^{-J_{ij}^2/2}. \tag{2}$$

• Bimodal ($\pm J$) distribution of bonds in which J_{ij} take the values ± 1 with equal probability

$$\mathcal{P}(J_{ij}) = \frac{1}{2}[\delta(J_{ij}-1) + \delta(J_{ij}+1)]. \tag{3}$$

In all cases that we study the mean of the distribution is zero. Since we set the standard deviation to be unity, the temperature is a dimensionless quantity.

B. Other models

We have also studied other models, although in less detail than the Gaussian and $\pm J$ models, in order to see if, by tuning parameters, we could eliminate the leading correction to scaling in any of them. These attempts have been unsuccessful; therefore we have collected less good statistics for these models than for the Gaussian and $\pm J$ distributions. Hence we shall not present results for these other models in detail, except in Sec. V D where we will do a global comparison of *all* the models studied to test for universality. These other models are

• Gaussian/bimodal distribution with $\Sigma_{\langle i,j \rangle} J_{ij}=0$: This model is the same as the model presented in Eqs. (2) and (3), but with the constraint that the sum of the J_{ij} is exactly zero.

• Correlated bonds: In this model the nearest-neighbor bonds have correlations. The probability distribution for the bonds is taken to be

$$\mathcal{P}(J_{ij}) \propto \exp\left[-\frac{1}{2}\sum_{\langle i,j \rangle} J_{ij}^2 - \lambda \sum_{\square,i} J_{i1}J_{i2}J_{i3}J_{i4} \right], \tag{4}$$

where the last term involves the product of the four bonds around an elementary plaquette of the lattice, and is summed over all plaquettes. It is this term which generates correlations in the bonds. We take $J_{ij}=\pm 1$, for which the first term in Eq. (4) is actually a constant. We generate correlated bonds by first performing a Monte Carlo simulation *on the bonds* using the Hamiltonian in Eq. (4). The bonds are then frozen and the spin simulation is carried out.

• Cosine disorder distribution: The bonds of the EA spin glass are chosen according to

$$\mathcal{P}(J_{ij}) = \frac{1}{2}\cos J_{ij} \quad \left[-\frac{\pi}{2} < J_{ij} < \frac{\pi}{2} \right]. \tag{5}$$

• Soft spins: In this model the spins S_i can take any length from $-\infty$ to $+\infty$ and the Hamiltonian is given by[29]

$$\mathcal{H} = -\sum_{\langle i,j \rangle} J_{ij} S_i S_j + \sum_i S_i^2 + \lambda \sum_i (S_i^2 - 1)^2, \tag{6}$$

where the bonds J_{ij} are Gaussian distributed and the parameter λ controls the average length of the spins. For $\lambda \to \infty$ we recover the Ising model with fixed-length spins.

C. Measured quantities

We measure different observables which, in the past, have proven to show a good signature of the phase transition.

First, we study the Binder cumulant[31] given by

$$g = \frac{1}{2}\left(3 - \frac{[\langle q^4\rangle_T]_{\rm av}}{[\langle q^2\rangle_T]^2_{\rm av}}\right), \tag{7}$$

where $\langle\cdots\rangle_T$ represents a thermal average, $[\cdots]_{\rm av}$ is a disorder average, and q is the spin overlap given by

$$q = \frac{1}{N}\sum_{i=1}^{N} S_i^\alpha S_i^\beta. \tag{8}$$

In the previous equation "α" and "β" represent two copies of the system with the same disorder. The Binder ratio is dimensionless and thus has the simple scaling form

$$g = \widetilde{G}(AL^{1/\nu}[\beta - \beta_c]), \tag{9}$$

where $\beta = 1/T$ and $\beta_{\rm c}$ is the inverse of the critical temperature. In addition to β_c, the "metric factor"[32] A is also nonuniversal, but, since A is included explicitly, the resulting scaling function $\widetilde{G}(x)$ *is universal*.[32] For the models studied here with no lattice anisotropy,[33–35] a universality class for finite-size scaling functions is specified by (i) the *bulk* universality class, (ii) the boundary conditions, and (iii) the sample shape. In this work we always use the same boundary conditions (periodic) and the same sample shape (cubic), so we expect the same function $\widetilde{G}(x)$ for models which lie in the same bulk universality class. According to Eq. (9), data for g for different sizes should intersect at T_c. Furthermore, the value of g at the intersection point, which is given by $\widetilde{G}(0)$ is also universal since the whole function $\widetilde{G}(x)$ is universal.

In addition, we study the finite-size correlation length ξ_L[24,25,36,37] defined by

$$\xi_L = \frac{1}{2\sin(k_{\rm min}/2)}\left[\frac{\chi_{\rm SG}(0)}{\chi_{\rm SG}(\mathbf{k}_{\rm min})} - 1\right]^{1/2}, \tag{10}$$

where $\mathbf{k}_{\rm min} = (2\pi/L, 0, 0)$ is the smallest nonzero wave vector. Here, the wave vector dependent spin-glass susceptibility is given by

$$\chi_{\rm SG}(\mathbf{k}) = \frac{1}{N}\sum_{i,j}[\langle S_i S_j\rangle_T^2]_{\rm av} e^{i\mathbf{k}\cdot(\mathbf{R}_i - \mathbf{R}_j)}. \tag{11}$$

Like the Binder ratio, the finite-size correlation length divided by the system size is a dimensionless quantity and so scales as

$$\frac{\xi_L}{L} = \widetilde{X}(AL^{1/\nu}[\beta - \beta_{\rm c}]), \tag{12}$$

in which the metric factor A is the *same*[32] as in Eq. (9). The reason the metric factors are the same is as follows: By hypothesis, the argument of *all* FSS functions is really L/ξ_∞, with *no* metric factor, where ξ_∞ is the bulk correlation length. In this form one has separate FSS functions for each side of the transition because $1/\xi_\infty = B_\pm|\beta - \beta_{\rm c}|^\nu$ vanishes in a singular manner at criticality. For example,

$$\frac{\xi_L}{L} = \widehat{X}_\pm(L/\xi_\infty) \tag{13}$$

$$= \widehat{X}_\pm(B_\pm L[\beta - \beta_{\rm c}]^\nu) \tag{14}$$

$$= \bar{X}_\pm(B_\pm^{1/\nu} L^{1/\nu}[\beta - \beta_c]), \tag{15}$$

in which $\widehat{X}_\pm$ and $\bar{X}_\pm$ are universal. Comparing Eq. (15) with Eq. (12), we see that there are universal, i.e., *distribution independent*, factors $c_\pm$ such that

$$A = c_+(B_+)^{1/\nu} = c_-(B_-)^{1/\nu}, \tag{16}$$

and therefore $\widetilde{X}$ and $\bar{X}$ are essentially the same functions, in the sense that

$$\widetilde{X}(u) = \begin{cases} \bar{X}_+(u/c_+) & (u > 0), \\ \bar{X}_-(u/c_-) & (u < 0). \end{cases} \tag{17}$$

If we repeat the argument for the Binder ratio g, we obtain

$$g = \bar{G}_\pm(B_\pm^{1/\nu} L^{1/\nu}[\beta - \beta_c]), \tag{18}$$

and choosing the same $c_\pm$ as in Eq. (16) we reproduce Eq. (9) with the *same* value for A as in Eq. (12).

The advantage of ξ_L/L over the Binder ratio g is that the Binder ratio, being restricted to the interval $g \in [0,1]$, does not have much room to "splay out" below T_c. Presumably because of this, the data for g in three dimensions depend only very weakly on the system size in this region.[20,23] However, the finite-size correlation length ξ_L/L does not have this constraint, and so the data for it splays out better at low temperatures, allowing for a more precise determination of the critical parameters.

Both g and ξ_L/L allow one to determine $T_{\rm c}$ and the critical exponent ν. However, to fully characterize the critical behavior of a system, a second critical exponent, e.g., η, is required.[38] Thus we also study the scaling of the spin-glass susceptibility $\chi_{\rm SG} \equiv \chi_{\rm SG}(\mathbf{k}=0)$ given by Eq. (11) with $\mathbf{k}=0$. Near criticality we expect

$$\chi_{\rm SG} = DL^{2-\eta}\widetilde{C}(AL^{1/\nu}[\beta - \beta_c]) \tag{19}$$

therefore allowing us to determine the critical exponent η. By separating out the nonuniversal amplitude D, the scaling function $\widetilde{C}$ is universal.

III. NUMERICAL DETAILS

The simulations are done using the parallel tempering Monte Carlo method.[39,40] For the Gaussian distribution we have tested equilibration with the method introduced in Ref. 41 where the energy computed directly is compared to the energy computed from the link overlap. The data for both quantities approach a limiting value from opposite directions. Once they agree, and other observables are independent of Monte Carlo steps, the system is in equilibrium. For the bimodal disorder distribution we use a multispin coded version of the algorithm which allows us to update 32 copies of the system at the same time. The aforementioned equilibration test cannot be applied to the bimodal spin glass. In this case we study how the results vary when the simulation time is successively increased by factors of 2 (logarithmic

TABLE II. Parameters of the simulations for Gaussian distributed disorder. N_{sa} is the number of samples, N_{sw} is the total number of Monte Carlo sweeps for each of the $2N_T$ replicas for a single sample, T_{min} is the lowest temperature simulated, and N_T is the number of temperatures used in the parallel tempering method for each system size L.

L	N_{sa}	N_{sw}	T_{min}	N_T
3	20000	32768	0.80	8
4	20000	20000	0.80	8
6	20000	40000	0.80	8
8	20000	50000	0.80	10
12	10000	655360	0.80	16
16	5000	1048576	0.80	33

binning). We require that the last three results for all observables agree within error bars.

Parameters of the simulation are presented in Tables II and III for the Gaussian and bimodal ($\pm J$) distributions, respectively.

IV. STATISTICAL ANALYSIS OF THE DATA

For the Binder ratio and finite-size correlation length we need to find the best choice of parameters, ν and β_c in order to collapse the data onto the scaling predictions of Eqs. (9) and (12), respectively. To do so we assume that the scaling function can be represented by a third-order polynomial $y(x)=c_0+c_1x+c_2x^2+c_3x^3$ and do a global fit to the six parameters $c_i,(i=0,\ldots,3)$, β_c, and ν. We also analyze results for χ_{SG}, for which there is a seventh parameter, the critical exponent η. We have performed these nonlinear fits in two ways: (i) a code based on the Levenberg-Marquardt algorithm,[42] and (ii) the statistics package R.[43] The same results have been obtained from both approaches.

It is also necessary to obtain error bars on the fit parameters. One has to be careful because, for a given size, all temperatures are simulated with the same disorder realization in the parallel tempering Monte Carlo method.[39,40] Hence the fitted data are correlated. We therefore have applied the following procedure: For each system size L with N_{sa} disorder realizations, a randomly selected bootstrap[44] sample of N_{sa} disorder realizations is generated. With this random sample, an estimate of the different observables (with bootstrap error bars) is computed for each temperature. We repeat this procedure $N_{boot}=1000$ times for each lattice size and then assemble N_{boot} complete data sets (each having results for every size) by combining the i-th bootstrap sample for each size for $i=1,\ldots,N_{boot}$. The finite-size scaling fit described above is then carried out on each of these N_{boot} sets, thus obtaining N_{boot} estimates of the fit parameters. Since the bootstrap sampling is done with respect to the disorder realizations which are statistically independent we can use a conventional bootstrap analysis to estimate statistical error bars on the fit parameters. These are equal to the standard deviation among the N_{boot} bootstrap estimates.

TABLE III. Parameters of the simulations, defined in Table II, for bimodal distributed disorder. The system sizes marked with an asterisk have been simulated with the more efficient multispin method.

L	N_{sa}	N_{sw}	T_{min}	N_T
3	40000	8000	0.82	16
4	40000	8000	0.82	16
6	40000	20000	0.82	16
8	30000	80000	0.82	16
12	15807	300000	0.82	18
16*	11360	128000	0.95	16
20*	9408	1280000	1.05	25
24*	8416	1280000	1.05	25

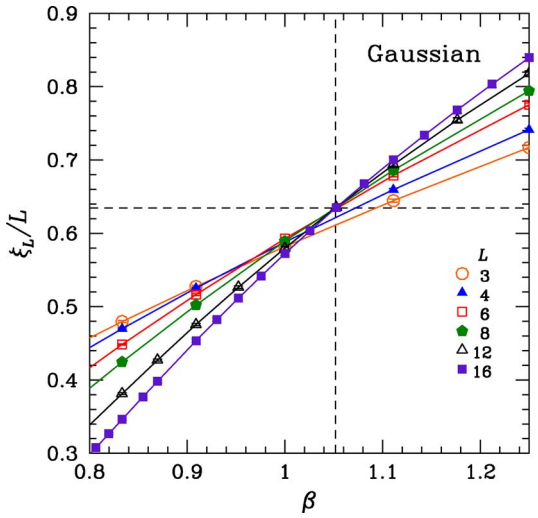

FIG. 2. (Color online) Finite-size correlation length ξ_L/L as a function of inverse temperature β for the three-dimensional Edwards-Anderson Ising spin glass with Gaussian disorder for several system sizes L. The data cross at $\beta_c^{-1}\simeq 0.951$. The dashed lines represent the optimal values obtained from a finite-size scaling for β_c and $\xi_L(\beta_c)/L$.

V. RESULTS

A. Gaussian-distributed random bonds

Figure 2 shows data for the finite-size correlation length as a function of the inverse temperature for different system sizes. The data for $L\geq 6$ intersect at (or very close to) a common point whereas the data for the smallest sizes, $L=3$ and 4 lie consistently too low in this region. The fact that sizes $L=3$ and 4 do not intersect at a common point clearly indicates that corrections to scaling are significant for these sizes. We were hoping to find other models where the trend would be the other way around (i.e., where the small-L data are too high) so that by fine tuning of parameters we could eliminate this correction to scaling. However, all the models studied (see Sec. II) had corrections of the same sign as shown in Fig. 2.

In scaling the data according to Eq. (12) in the way discussed in Sec. IV, we omit sizes $L=3$ and 4 because these

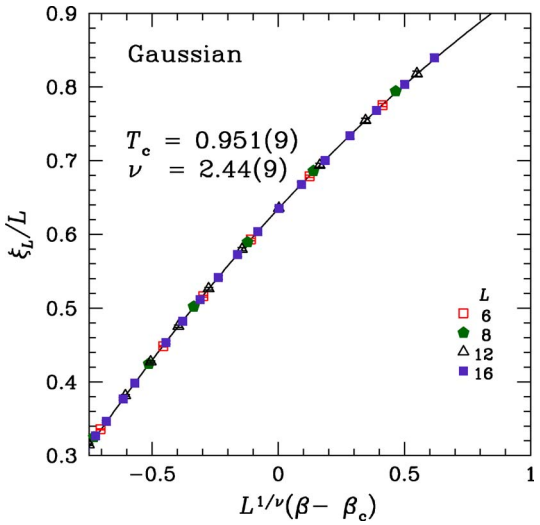

FIG. 3. (Color online) Finite-size scaling analysis of ξ_L/L for the Ising spin glass with Gaussian bonds according to Eq. (12). The sizes are $6 \leq L \leq 16$. The solid line is the third-order polynomial used in the fit, see Sec. IV.

data are clearly affected by corrections to scaling, and Fig. 3 shows the resulting plot for sizes $L \geq 6$. The overall fit is very satisfactory and gives the critical parameters shown in Table IV.

In Fig. 4 we show data for the Binder ratio, Eq. (7), as a function of the inverse temperature β. The data cross at $\beta_c^{-1} \simeq 0.931$. Note that for $\beta > \beta_c$ the data do not splay very well thus making it difficult to determine the critical temperature accurately.

Using the analysis presented in Sec. IV we have obtained the best fit, shown in Table IV, and present the scaling plot of the Binder ratio in Fig. 5. For the analysis we have only considered $L \geq 6$.

Overall, we expect that the analysis of ξ_L/L gives more accurate results than that for g, because the data for g do not splay out much below T_c, and so our best results for T_c and ν are those for ξ_L/L, i.e.,

$$T_c = 0.951(9), \quad \nu = 2.44(9) \quad \text{(Gaussian)}. \tag{20}$$

We emphasize that the error bars quoted in this paper are only statistical. There are also systematic errors, which are hard to estimate for the range of sizes that can be studied. We discuss systematic errors below in more detail, especially in Secs. V C and VI. It is gratifying that the results obtained from the analysis of g, namely, $T_c = 0.931(17)$, $\nu = 2.67(17)$ are (just) consistent with these. In addition to exponents, the values of ξ_L/L and g at T_c are also expected to be universal. These are given by the appropriate values of c_0 in Table IV:

$$\frac{\xi_L(T_c)}{L} = 0.635(9), \quad g(T_c) = 0.760(70) \quad \text{(Gaussian)}. \tag{21}$$

Unfortunately, the situation for the analysis of the spin-glass susceptibility data is less gratifying. The scaling plot for the spin-glass susceptibility is shown in Fig. 6. For consistency with the other plots the horizontal axis in this figure is β. However, the method of fitting (third-order polynomial) works best, in this case, for a fit using T. Hence Fig. 6 indicates the fit parameters from the T fit.

TABLE IV. Summary of critical parameters for a Gaussian disorder distribution estimated by scaling the data. Scaling has been done in $(\beta - \beta_c)$ except for the spin-glass susceptibility for which the data has been scaled with $(T - T_c)$. In the table below, T_c is the critical temperature, and η and ν are critical exponents. The quantity c_0 is the zeroth-order coefficient of the fitting polynomial and corresponds to the value of a given observable at criticality. χ^2 represents the chi-squared value for the finite-size scaling fitting function (Ref. 42). For comparison the number of data points used in the fit is 25. For the fit using the scaling form of Ref. 28 the value of T_c is fixed to be that obtained from ξ_L/L.

ξ_L/L	Estimate	Error
c_0	0.6346	0.0090
T_c	0.9508	0.0089
ν	2.4370	0.0924
χ^2	11.7859	10.2696
g	Estimate	Error
c_0	0.7600	0.0068
T_c	0.9310	0.0137
ν	2.6761	0.1662
χ^2	17.7245	14.0111
χ_{SG}	Estimate	Error
T_c	0.9489	0.0264
ν	1.4859	0.0602
η	−0.3733	0.0483
χ^2	12.8776	8.0025
χ_{SG} (scaling as in Ref. 28)	Estimate	Error
T_c	0.9508	0.0089
ν	2.7767	0.0249
η	−0.3716	0.0055
χ^2	18.3403	12.6776

The results of the fit are

$$T_c = 0.949(26), \quad \nu = 1.49(6), \quad \eta = -0.37(5). \tag{22}$$

The value for T_c agrees within the error bars with those from ξ_L/L and g, but the value for ν is in strong disagreement. Disagreements between exponents obtained in different ways are presumably due to corrections to FSS, but the size of the difference here is surprisingly large. In Sec. V C we shall revisit the problem of the surprisingly low value for ν obtained from χ_{SG}.

B. Bimodal-distributed random bonds

We show data for ξ_L/L in Fig. 7. It is fairly similar to the data for the Gaussian distribution in that the larger sizes show a common intersection, but the data for the smaller

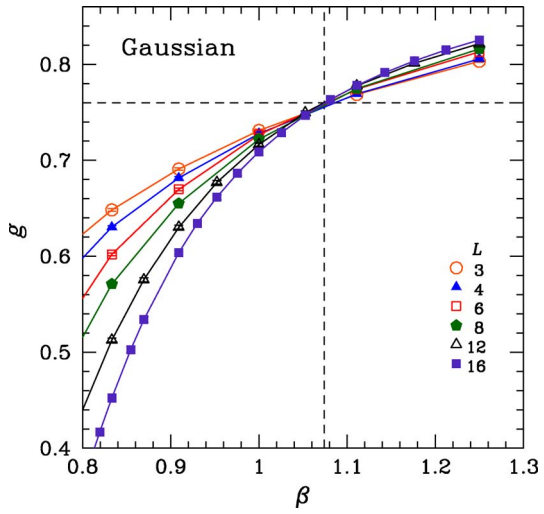

FIG. 4. (Color online) Binder ratio g, defined in Eq. (7), as a function of inverse temperature β for the three-dimensional Edwards-Anderson Ising spin glass with Gaussian bonds. The data cross at $\beta_c^{-1} \simeq 0.931$. The dashed lines represent the optimal values obtained from a finite-size scaling for β_c and $g(\beta_c)$.

sizes, $L=3$ and 4, are lower, showing that these sizes are affected by corrections to FSS. Hence we only use sizes $6 \leq L \leq 24$ in the scaling plot which is shown in Fig. 8. Parameters obtained from the fits are shown in Table V.

Figure 9 shows data for the Binder ratio, Eq. (7), for different system sizes L as a function of the inverse temperature β. The corresponding scaling plot is shown in Fig. 10.

The fit parameters obtained from ξ_L/L are

$$T_c = 1.120(4), \quad \nu = 2.39(5) \quad (\pm J). \tag{23}$$

Those obtained from g, namely, $T_c=1.088(6)$, $\nu=2.79(11)$ disagree somewhat, but, as also discussed above, we feel that

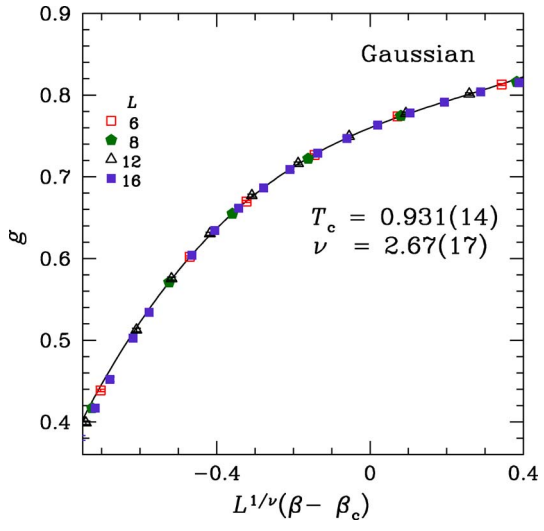

FIG. 5. (Color online) Finite-size scaling analysis of the data for the Binder ratio g according to Eq. (9) for the three-dimensional Ising spin glass with Gaussian disorder. The scaling analysis is performed for $L \geq 6$ and the solid line represents the best fit to the data from the finite-size scaling analysis.

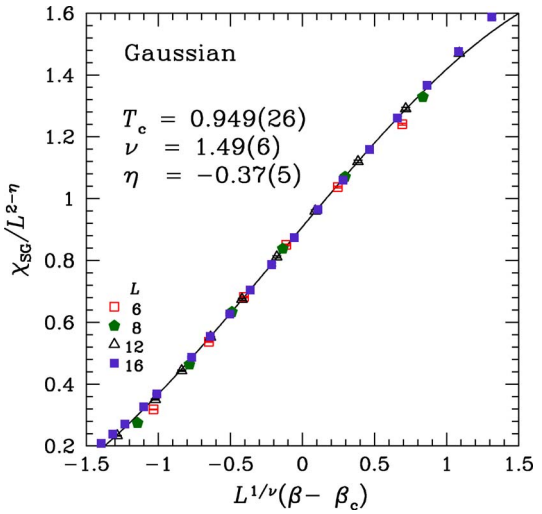

FIG. 6. (Color online) Finite-size scaling of the spin-glass susceptibility χ_{SG} according to Eq. (19) for Gaussian disorder. In fact, the method of scaling worked better when using T rather than β and the fit parameters shown are for the T fit. However, we show the resulting scaling plot using β for consistency with the other plots. The scaling analysis is performed for $L \geq 6$.

those for ξ_L/L are more reliable because the data for ξ_L/L splay out more below T_c.

The values of ξ_L/L and g at T_c are given by the appropriate values of c_0 in Table V:

$$\frac{\xi_L(T_c)}{L} = 0.627(4), \quad g(T_c) = 0.763(3) \quad (\pm J). \tag{24}$$

A scaling plot for χ_{SG} is shown in Fig. 11. The best fit (using T rather than β) gives

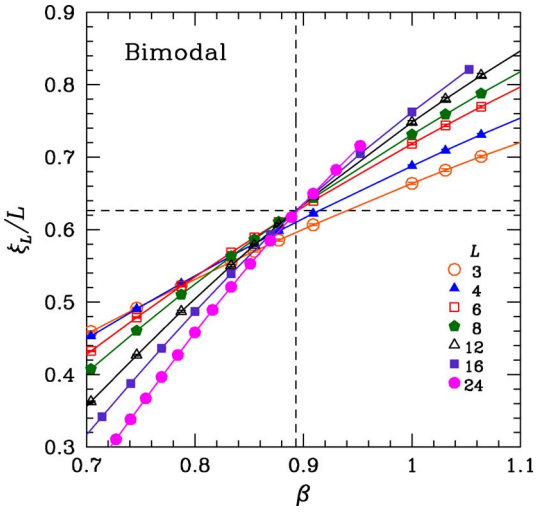

FIG. 7. (Color online) Finite-size correlation length ξ_L/L as a function of inverse temperature β for the three-dimensional Edwards-Anderson Ising spin glass with $\pm J$ bonds for several system sizes L. The data cross at $\beta_c^{-1} \simeq 1.12$. The dashed lines represent the optimal values obtained from a finite-size scaling for β_c and $\xi_L(\beta_c)/L$.

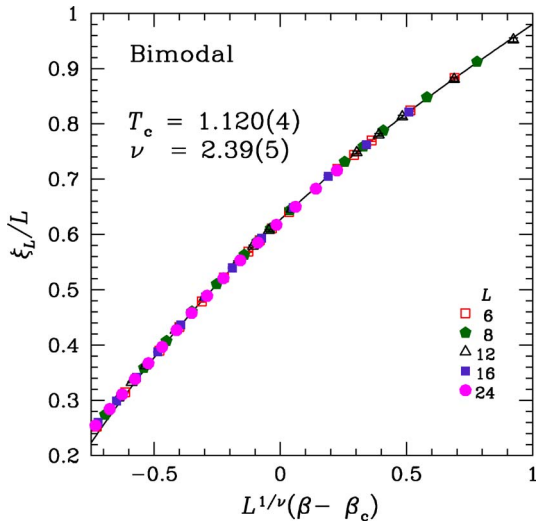

FIG. 8. (Color online) Finite-size scaling analysis of ξ_L/L for the Ising spin glass with $\pm J$ bonds according to Eq. (12). The scaling analysis is performed for $L \geq 6$.

$$T_c = 1.104(9), \quad \nu = 1.57(3), \quad \eta = -0.395(17). \quad (25)$$

The value of T_c differs from that obtained from ξ_L/L, in Eq. (23) by rather more than the error bars. If we fix T_c to be that obtained from ξ_L/L we find

$$\nu = 1.527(8), \quad \eta = -0.368(24). \quad (26)$$

The value of η obtained in this way is consistent with that in the unconstrained fit in Eq. (25). The value of ν is slightly different from that in Eq. (25), but more importantly, both these values of ν obtained from χ_{SG} are considerably smaller than those obtained from ξ_L/L and g. This is the same situation than found for the Gaussian distribution. Interestingly, the values of ν from χ_{SG} for the two distributions agree quite well *with each other*.

We argue that the most reliable quantity to analyze is ξ_L/L because this has clean intersections with significant splaying out below T_c. The results for the exponent ν, shown in Eqs. (20) and (23), for the Gaussian and $\pm J$ distributions agree well within the error bars, which supports universality. Further support for universality comes from the agreement in the values of ξ_L/L and g at the critical point, shown in Eqs. (21) and (24). We also note the agreement in the values of η from Eqs. (22) and (25) or (26).

C. Alternative analysis of χ_{SG}

The main unresolved issue is the large difference in the values of ν obtained from the spin-glass susceptibility compared with those obtained from ξ_L/L and g. Recently, Campbell *et al.*[28] have claimed that the difference is much diminished if one uses an alternative scaling form. They propose that the scaling region will be larger, so one can incorporate data for a larger range of temperature, if the behavior as $T \to \infty$ is consistent with the scaling function. To be precise, they propose that

$$g = \tilde{G}[(LT)^{1/\nu}(1 - (T_c/T)^2)], \quad (27)$$

TABLE V. Summary of critical parameters for a bimodal disorder distribution estimated by scaling the data. The scaling is done in $(\beta - \beta_c)$ except for the data for the spin-glass susceptibility where the scaling is done in $(T - T_c)$. For further details see the caption of Table IV. The number of data points used in the fits is 48. In the fit for χ_{SG} using the scaling form of Ref. 28 the value of T_c is fixed to be that obtained from ξ_L/L.

ξ_L/L	Estimate	Error
c_0	0.6265	0.0036
T_c	1.1199	0.0037
ν	2.3900	0.0514
χ^2	52.8369	28.3532
g	Estimate	Error
c_0	0.7626	0.0029
T_c	1.0881	0.0062
ν	2.7937	0.1103
χ^2	60.5020	30.2953
χ_{SG}	Estimate	Error
T_c	1.1040	0.0097
ν	1.5721	0.0251
η	−0.3954	0.0168
χ^2	88.2526	31.8466
χ_{SG} (scaling as in Ref. 28)	Estimate	Error
T_c	1.1199	0.0037
ν	2.7376	0.0166
η	−0.3663	0.0166
χ^2	83.6070	36.7894

$$\frac{\xi_L}{L} = \tilde{X}[(LT)^{1/\nu}(1 - (T_c/T)^2)], \quad (28)$$

$$\chi_{SG} = (LT)^{2-\eta}\tilde{C}[(LT)^{1/\nu}(1 - (T_c/T)^2)], \quad (29)$$

where we have not included explicitly the metric factors. Asymptotically, for $L \to \infty$ and $(T - T_c) \to 0$, these expressions are equivalent to the standard forms that we have used, Eqs. (9), (12), and (19). Thus the difference between the expressions proposed by Campbell *et al.* and the standard expressions is only in the corrections to scaling.

In both the original scaling forms and the modified form of Campbell *et al.*, T_c is located by intersections of data for ξ_L/L and g of different sizes. Thus we do not expect the estimates of T_c to be very different in the two approaches. Furthermore, if we restrict data to the region close to T_c, the data collapse involves mainly the derivative of the data with respect to temperature at T_c. For ξ_L/L and g, both the original and modified form predict that the temperature derivative is proportional to $L^{1/\nu}$. Hence, for ξ_L/L and g, we also do not expect very different values for ν from the two scaling forms. These expectations are confirmed by our analysis. Using Eqs. (27) and (28), we find values for T_c and ν which

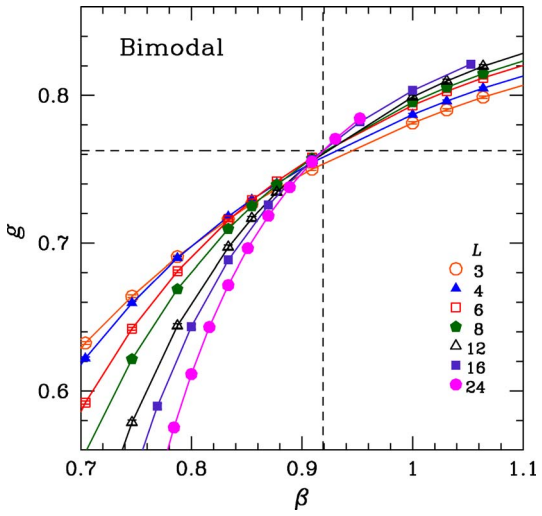

FIG. 9. (Color online) Binder ratio g as a function of inverse temperature β for the three-dimensional Edwards-Anderson Ising spin glass with $\pm J$ bonds for several system sizes L. The data cross at $\beta_c^{-1} \simeq 1.088$. The dashed lines represent the optimal values obtained from a finite-size scaling for β_c and $g(\beta_c)/L$.

agree, within the error bars, with those described above in Secs. V A and V B which used the standard scaling forms. It is possible that scaling may work for data over a larger range of $(T-T_c)$, at least above[45] T_c, using Eqs. (27) and (28), but we have not investigated this in detail.

However, the situation for χ_{SG} is quite different, because of the factor of $T^{2-\eta}$ in front of the scaling function in Eq. (29), since

$$\frac{1}{\chi_{\mathrm{SG}}} \frac{d\chi_{\mathrm{SG}}}{dT}\bigg|_{T_c} = aL^{1/\nu} + b, \tag{30}$$

where a and b depend on T_c and the value of the scaling function and its derivative at zero argument, but not on L.

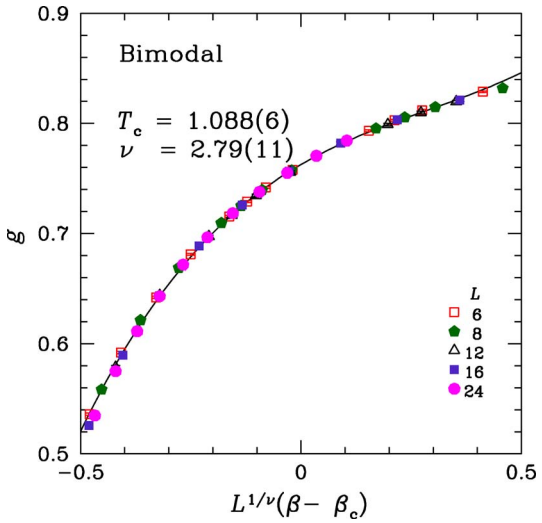

FIG. 10. (Color online) Finite-size scaling analysis of the data for the Binder ratio g according to Eq. (9) for the three-dimensional Ising spin glass with $\pm J$ bonds. The sizes used are $6 \leq L \leq 24$.

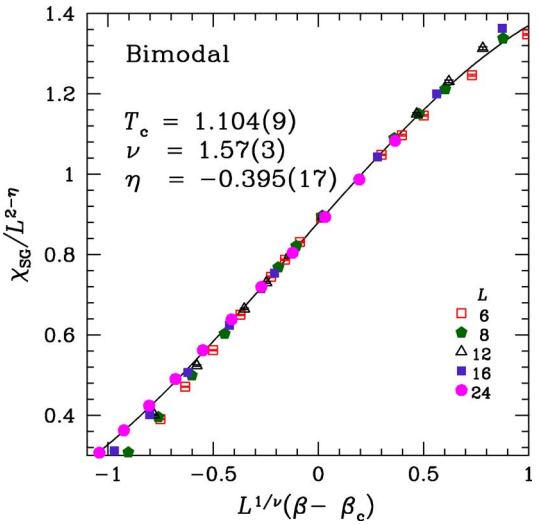

FIG. 11. (Color online) Finite-size scaling of the spin-glass susceptibility χ_{SG} according to Eq. (19) for the three-dimensional Ising spin glass with $\pm J$ bonds. As for the corresponding plot for the Gaussian distribution, Fig. 6, the fit is actually done in T, but the plot is given as a function of β for consistency with the other plots. The scaling analysis is performed for $L \geq 6$.

The factor of b arises from the T dependence of the prefactor *outside* the scaling function in Eq. (29), and does not occur in the analogous expressions for ξ_L/L and g in Eqs. (28) and (27). For $L \to \infty$, the $L^{1/\nu}$ term in Eq. (30) dominates and we recover the same behavior as in the standard scaling form. However, for the small sizes that can be studied numerically, the factor of b gives a significant correction to scaling *especially since* $1/\nu$ *is small*. This is why Campbell *et al.*[28] found a large difference in the value of ν obtained from χ_{SG} using their scaling compared with conventional finite-size scaling.

We also find a large difference. If we fix T_c to be the value obtained from ξ_L/L we obtain, from Eq. (29)

$$\nu = 2.777(25), \quad \eta = -0.372(6) \quad \text{(Gaussian)}, \tag{31}$$

$$\nu = 2.738(17), \quad \eta = -0.366(3) \quad (\pm J), \tag{32}$$

see also Tables IV and V. These values for ν are *considerably* larger than those found from the standard analysis discussed in Secs. V A and V B. They are even somewhat larger than those found from ξ_L/L, although they agree better with the ξ_L/L values than those found from χ_{SG} using the standard analysis. The fact that we, like Ref. 28, obtain very different values for ν from χ_{SG} depending on the form of the scaling function used, tells us that corrections to scaling can be very important in spin glasses for the range of sizes that can be simulated. We note, however, that the two estimates in Eqs. (31) and (32) agree well *with each other*, so we still find no evidence for lack of universality.

D. Global comparisons of all the models

We have computed two dimensionless quantities ξ_L/L and g, which intersect at a finite value at the critical temperature. In the previous parts of this section, we have plotted both of

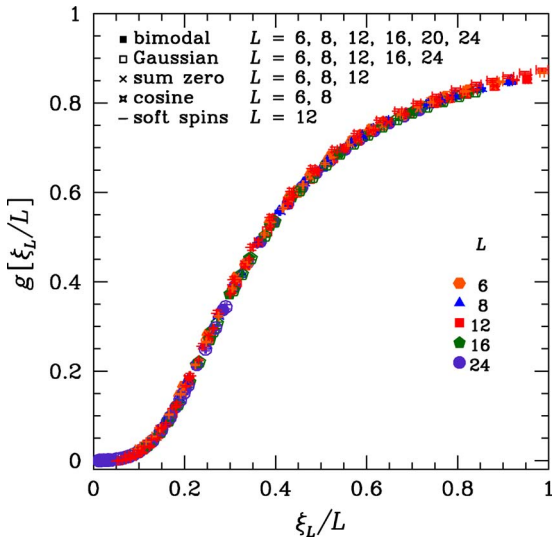

FIG. 12. (Color online) Binder ratio g as a function of the finite-size correlation length ξ_L/L for several system sizes $L \geq 6$ and for all models described in Sec. II. All data collapse onto a universal curve, thus providing clear evidence that spin glasses obey universality. Different system sizes are labeled with different colors, and different models use different types of symbols as indicated.

them against β. It turns out also to be useful to plot one of them *against the other*.[46,47] According to Eq. (12), $AL^{1/\nu}[\beta - \beta_c] = \tilde{X}^{-1}(\xi_L/L)$ and so, from Eq. (9), we can write

$$g = \hat{G}(\xi_L/L), \tag{33}$$

where $\hat{G}$ is a universal function. Note that there are *no* non-universal metric factors in this expression. Hence data for *all* the models described in Sec. II should collapse when g is plotted against ξ_L/L. This works very well as shown in Fig. 12 which includes sizes $L \geq 6$. Figure 12 provides additional *very strong evidence for universality* in spin glasses.

VI. SUMMARY AND CONCLUSIONS

We have studied numerically the phase transition in a variety of Ising spin-glass models in three dimensions, to test for universality. Our most detailed simulations are on nearest-neighbor models with Gaussian and $\pm J$ interactions, and our results for them are summarized in Tables IV and V. A comparison shows that corresponding estimates for the exponents ν and η agree well, as do the values of ξ_L/L and g at criticality (labeled c_0). This supports universality, as does the plot of g against ξ_L/L, Fig. 12, where data for *all* the models studied (not just the Gaussian and $\pm J$ models) collapse onto a single universal curve.

The main unresolved issue is the large difference between the values for ν obtained from ξ_L/L or g on the one hand and $\chi_{\rm SG}$ on the other. This is presumably due to systematic errors coming from corrections to scaling, but unfortunately we have not been able to incorporate corrections in our analysis since we do not have data with sufficient precision over a sufficiently large range of sizes. The errors quoted in this paper are statistical errors only; systematic errors are not included. Evidence for strong corrections was found explicitly in Sec. V C, where we used a scaling form for $\chi_{\rm SG}$ proposed in Ref. 28 which differs from the standard form only in corrections to scaling. From this scaling form, we obtain an estimate for ν from our data for $\chi_{\rm SG}$ which is very different from that obtained from $\chi_{\rm SG}$ using the standard analysis. This large difference in the values of ν from the two methods of analysis does not occur, however, for our data for g and ξ_L/L.

Overall, we have found no evidence for lack of universality, but have found evidence for strong corrections to scaling. We suspect that the dynamical data of Refs. 3–7, which was interpreted to show lack of universality, more likely shows evidence for corrections to scaling.

ACKNOWLEDGMENTS

We would like to thank K. Binder, I. A. Campbell, T. Jörg, K. Hukushima, D. P. Landau, H. Takayama, M. Troyer, and D. Würtz for discussions. In particular, we would like to thank T. Jörg for pointing out the usefulness of plotting our data in the way shown in Fig. 12. A.P.Y. acknowledges support from the National Science Foundation under NSF Grant No. DMR 0337049. The simulations were performed on the Asgard, Hreidar, and Gonzales clusters at ETH Zürich. We would like to thank K. Tran for carefully reading the manuscript.

[1] K. Binder and A. P. Young, Rev. Mod. Phys. **58**, 801 (1986).
[2] D. Daboul, I. Chang, and A. Aharony, Eur. Phys. J. B **41**, 231 (2004).
[3] L. W. Bernardi, S. Prakash, and I. A. Campbell, Phys. Rev. Lett. **77**, 2798 (1996).
[4] P. O. Mari and I. A. Campbell, Phys. Rev. E **59**, 2653 (1999).
[5] P. O. Mari and I. A. Campbell cond-mat/0111174 (unpublished).
[6] M. Henkel and M. Pleimling, Europhys. Lett. **69**, 524 (2005).
[7] M. Pleimling and I. A. Campbell, Phys. Rev. B **72**, 184429 (2005).
[8] Reference 6 claims only that universality is violated out of equilibrium.
[9] S. F. Edwards and P. W. Anderson, J. Phys. F: Met. Phys. **5**, 965 (1975).
[10] T. Jörg, preceding paper, Phys. Rev. B **73**, 224431 (2006).
[11] J. Houdayer, Eur. Phys. J. B **22**, 479 (2001).
[12] F. P. Toldin, A. Pelissetto, and E. Vicari, J. Stat. Mech.: Theory Exp. 2006, P06002.
[13] A. T. Ogielski and I. Morgenstern, Phys. Rev. Lett. **54**, 928 (1985).

[14] A. T. Ogielski, Phys. Rev. B **32**, 7384 (1985).
[15] W. L. McMillan, Phys. Rev. B **31**, 340 (1985).
[16] R. R. P. Singh and S. Chakravarty, Phys. Rev. Lett. **57**, 245 (1986).
[17] A. J. Bray and M. A. Moore, Phys. Rev. B **31**, 631 (1985).
[18] R. N. Bhatt and A. P. Young, Phys. Rev. Lett. **54**, 924 (1985).
[19] R. N. Bhatt and A. P. Young, Phys. Rev. B **37**, 5606 (1988).
[20] N. Kawashima and A. P. Young, Phys. Rev. B **53**, R484 (1996).
[21] D. Iñiguez, G. Parisi, and J. J. Ruiz-Lorenzo, J. Phys. A **29**, 4337 (1996).
[22] B. A. Berg and W. Janke, Phys. Rev. Lett. **80**, 4771 (1998).
[23] E. Marinari, G. Parisi, and J. J. Ruiz-Lorenzo, Phys. Rev. B **58**, 14852 (1998).
[24] M. Palassini and S. Caracciolo, Phys. Rev. Lett. **82**, 5128 (1999).
[25] H. G. Ballesteros, A. Cruz, L. A. Fernandez, V. Martin-Mayor, J. Pech, J. J. Ruiz-Lorenzo, A. Tarancon, P. Tellez, C. L. Ullod, and C. Ungil, Phys. Rev. B **62**, 14237 (2000).
[26] P. O. Mari and I. A. Campbell, Phys. Rev. B **65**, 184409 (2002).
[27] T. Nakamura, S.-i. Endoh, and T. Yamamoto, J. Phys. A **36**, 10895 (2003).
[28] I. A. Campbell, K. Hukushima, and H. Takayama, cond-mat/0603453 (unpublished).
[29] M. Hasenbusch, J. Phys. A **32**, 4851 (1999).
[30] K. D. D. Beach, L. Wang, and A. W. Sandvik, cond-mat/0505194 (unpublished).
[31] K. Binder, Phys. Rev. Lett. **47**, 693 (1981).
[32] V. Privman and M. E. Fisher, Phys. Rev. B **30**, 322 (1984).
[33] X. S. Chen and V. Dohm, Phys. Rev. E **70**, 056136 (2004).
[34] X. S. Chen and V. Dohm, Phys. Rev. E **71**, 059901(E) (2005).
[35] W. Selke and L. N. Shchur, J. Phys. A **38**, L739 (2005).
[36] F. Cooper, B. Freedman, and D. Preston, Nucl. Phys. B **210**, 210 (1982).
[37] V. Martín-Mayor, A. Pelissetto, and E. Vicari, Phys. Rev. E **66**, 026112 (2002).
[38] J. M. Yeomans, *Statistical Mechanics of Phase Transitions* (Oxford University Press, Oxford, 1992).
[39] K. Hukushima and K. Nemoto, J. Phys. Soc. Jpn. **65**, 1604 (1996).
[40] E. Marinari, G. Parisi, J. Ruiz-Lorenzo, and F. Ritort, Phys. Rev. Lett. **76**, 843 (1996).
[41] H. G. Katzgraber, M. Palassini, and A. P. Young, Phys. Rev. B **63**, 184422 (2001).
[42] W. H. Press, S. A. Teukolsky, W. T. Vetterling, and B. P. Flannery, *Numerical Recipes in C* (Cambridge University Press, Cambridge, 1995).
[43] R Core Team (R Manuals), URL http://cran.r-project.org
[44] We pick N_{sa} samples out of our set of N_{sa} *with replacement*, so the same sample might be picked more than once. For large N_{sa}, the number of times a sample is picked is a Possion distribution with mean unity.
[45] Although it is plausible that the data may scale over a wider range of $(T-T_c)$ *above* T_c in the analysis of Ref. 28, since their method is designed such that the high-T behavior is compatible with the scaling function, it is not clear to us that the data should also scale over a wider range of $(T-T_c)$ *below* T_c.
[46] J.-K. Kim, A. J. F. de Souza, and D. P. Landau, Phys. Rev. E **54**, 2291 (1996).
[47] T. Jörg (private communication).